ClO infrared emission spectrum retrieval using the Michelson Interferometer for Passive Atmospheric Sounding (MIPAS)

Jim Robinson*

14th April, 2000

Abstract

Infrared emission spectra for atmospheric profiles consisting of 17 gases, including chlorine monoxide (ClO) corresponding to maximum observed levels (Antarctic winter), were simulated using the Reference Forward Model (RFM) developed at the University of Oxford for the forthcoming European Space Agency (ESA) Michelson Interferometer for Passive Atmospheric Sounding (MIPAS) mission. Jacobians (Weighting Functions) were calculated using small perturbations to the ClO profile to determine how accurately information about the ClO Volume Mixing Ratio (VMR) may be retrieved from MIPAS, corrections having been made for Field-Of-View (FOV) effects as well as noise apodisation. It was found that ClO profile information for Antarctic winter conditions may be retrieved within typical 1σ error bars of $\sim$50% (corresponding to $\sim$1.0 ppbv) at best, at altitudes of 17 km and 20 km. At 23km, the 1σ bars were $\sim$80%, although it may be possible to achieve improved accuracy by averaging a number of single spectra. Outside the $\sim$17–23 km range, simulated error bars became too large for any useful measurements to be made. Furthermore, ClO is not sufficiently abundant at midlatitudes for useful profile information to be obtained.

1 Introduction

In the late 1980s it became clear that ozone was being depleted over the polar regions due to chemical processes following the decomposition of man-made chlorofluorocarbons (CFCs). Stratospheric ozone normally provides very effective shielding against ultraviolet radiation, which has damaging effects on humans and animals. It is therefore important to be able to monitor levels of both stratospheric ozone and other gases which are involved in its destruction. One of these gases is the free radical chlorine monoxide (ClO).

ClO is difficult to detect because of its low abundance and weak emission spectrum which tends to be swamped by infra-red radiation from other emitters. ClO has been observed before from ground stations [1], aircraft [2], stratospheric balloons [3] and satellites [4]—as described in Section 4. However, it is not yet clear whether the MIPAS instrument due to be launched on Envisat-1 will be able to detect it. Some previous analysis [5] has been carried out, but was completed before MIPAS had been constructed and hence before details of MIPAS's actual Noise Equivalent Spectral Radiance (NESR) and spectral resolution were known from instrument testing. This previous work also lacked the full statistical retrieval analysis adopted here. The purpose of this study is therefore to determine whether remote sounding of ClO will be possible in view of all that is now known about MIPAS.

2 The MIPAS Instrument

MIPAS is due to be launched by the European Space Agency (ESA) on Envisat-1 in late 2001 [6]. Envisat-1 will be a sun-synchronous, polar-orbiting Earth observation satellite, intended to provide data over a five-year period.

MIPAS is a high-resolution Fourier transform spectrometer, designed to make measurements of gaseous emission spectra at the Earth's limb. Versions of MIPAS have already been operated from the ground, aircraft and stratospheric balloons. However, MIPAS on Envisat-1 will be the first spaceborne high spectral resolution limb emission spectrometer which covers the whole mid infrared.

One of the objectives of MIPAS is to make simul-

* St. Catherine's College, University of Oxford, UK.

taneous and global measurements of geophysical parameters in the middle atmosphere, including temperature. In particular, the instrument is designed to observe emission lines due to the six major species O_3, H_2O, HNO_3, CH_4, N_2O and NO_2 with the aim of generating climatology data and improving our understanding of stratospheric chemistry. The retrieval of these parameters is to be performed in Near Real Time (NRT). Further products will be able to be retrieved non-operationally, particularly by scientific institutions such as the Department of Atmospheric, Oceanic and Planetary Physics (AOPP) at the University of Oxford.

MIPAS's spectral coverage is in the range 14.6 μm to 4.15 μm or 685 cm^{-1} to 2410 cm^{-1} in five wavelength bands. Its design sensitivity is better than 50nW/cm^2 sr cm^{-1}, decreasing to 4.2nW/cm^2 sr cm^{-1} at the short wavelength side. Ground tests have indicated a noise performance a factor of two better than this.

3 Chlorine Chemistry in the Stratosphere

3.1 The Chlorine Cycle

Free chlorine (Cl) atoms are produced by the destruction of CFCs and other chlorine source gases via ultraviolet photolysis in the stratosphere.

The stratospheric chlorine cycle and its coupling to the nitrogen cycle and the less important bromine cycle is extremely complicated, comprising dozens of reactions, but there are four rapid reactions involving Cl, which are the most significant on short time-scales [7].

Chlorine monoxide (ClO) is created and destroyed in a catalytic cycle involving monatomic oxygen:

$$\mathrm{Cl} + \mathrm{O_3} \rightarrow \mathrm{ClO} + \mathrm{O_2} \quad (1)$$
$$\mathrm{ClO} + \mathrm{O} \rightarrow \mathrm{Cl} + \mathrm{O_2}. \quad (2)$$

Coupling to the nitrogen cycle is provided by the reaction:

$$\mathrm{ClO} + \mathrm{NO} \rightarrow \mathrm{Cl} + \mathrm{NO_2}. \quad (3)$$

ClO is also destroyed by photolysis:

$$\mathrm{ClO} + \mathrm{h}\nu \rightarrow \mathrm{Cl} + \mathrm{O}. \quad (4)$$

Reactions (1)–(4) largely determine the concentration ratio [ClO]:[Cl]. Interconversion of Cl and ClO typically occurs on a time scale of one minute at 30km.

Note that (2) and (3) require the reagents O and NO respectively, which are generated by photolysis. Also, (4) is dependent upon solar illumination.

There are also reactions which convert Cl and ClO to reservoir species. These play an important role in determining the magnitude of the [ClO+Cl] sum over time scales longer than a day.

Further reactions yield hydrochloric acid (HCl):

$$\mathrm{Cl} + \mathrm{CH_4} \rightarrow \mathrm{CH_3} + \mathrm{HCl} \quad (5)$$
$$\mathrm{Cl} + \mathrm{HO_2} \rightarrow \mathrm{HCl} + \mathrm{O_2} \quad (6)$$
$$\mathrm{Cl} + \mathrm{H_2} \rightarrow \mathrm{HCl} + \mathrm{H} \quad (7)$$
$$\mathrm{Cl} + \mathrm{H_2O_2} \rightarrow \mathrm{HCl} + \mathrm{HO_2}. \quad (8)$$

HCl is the longest-lived and consequently most abundant Cl reservoir species, having a lifetime of about a month.

HCl is broken down largely by reaction with OH:

$$\mathrm{OH} + \mathrm{HCl} \rightarrow \mathrm{H_2O} + \mathrm{Cl} \quad (9)$$

which returns Cl to its active form.

Another reservoir species, $\mathrm{ClONO_2}$, is generated in the reaction:

$$\mathrm{ClO} + \mathrm{NO_2} + M \rightarrow \mathrm{ClONO_2} + M. \quad (10)$$

where M is any molecule, required for momentum conservation.

$\mathrm{ClONO_2}$ can undergo photolysis or react with O atoms:

$$\mathrm{ClONO_2} + \mathrm{h}\nu \rightarrow \mathrm{Cl} + \mathrm{NO_3} \quad (11)$$
$$\rightarrow \mathrm{ClO} + \mathrm{NO_2} \quad (12)$$
$$\mathrm{O} + \mathrm{ClONO_2} \rightarrow \mathrm{products} \quad (13)$$

which return Cl to active forms.

The lifetime of $\mathrm{ClONO_2}$ is dependent on the intensity of UV light present, varying from about six hours in the midlatitude lower stratosphere to about an hour at 40 km.

HOCl is produced too:

$$\mathrm{HO_2} + \mathrm{ClO} \rightarrow \mathrm{HOCl} + \mathrm{O_2}. \quad (14)$$

However, HOCl undergoes fairly rapid photolysis, on the time scale of less than one hour throughout the stratosphere:

$$\mathrm{HOCl} + \mathrm{h}\nu(\lambda < 301\mathrm{nm}) \rightarrow \mathrm{ClO} + \mathrm{H} \quad (15)$$
$$\mathrm{HOCl} + \mathrm{h}\nu(\lambda < 503\mathrm{nm}) \rightarrow \mathrm{Cl} + \mathrm{OH} \quad (16)$$

returning Cl to active forms.

3.2 Heterogeneous Chemistry

It should also be noted that reactions can occur on or in aerosol particles, such as Polar Stratospheric Clouds (PSCs) and liquid water/suphuric acid droplets. This is known as Heterogeneous Chemistry. These reactions can be of great importance in converting inactive Cl compounds to active forms of Cl in the polar stratosphere.

Two types of PSCs are distinguishable [8]. Type I PSCs form at temperatures below about 197 K and consist of condensed HNO_3 and H_2O. Type II PSCs form below the frost point (187 K) and are mainly made up of H_2O ice. Both these types are apparently confined to polar regions within the polar vortices, occurring during winter and early spring. The presence of PSCs can decisively affect stratospheric conditions.

For example, the reaction

$$N_2O_5(g) + H_2O(l) \quad \rightarrow \quad 2HNO_3(g), \qquad (17)$$

which occurs on sulphate aerosols, leads to the conversion of N_2O_5 to HNO_3. This denitrification causes a reduction in the abundance of NO_2 because N_2O_5 is a nighttime reservoir for NO_2. In turn, this leads to an increase in the ratio of ClO to $ClONO_2$ (as can be seen from reaction (10)), enhancing the ability of Cl to destroy ozone.

Also, at low temperatures, the hydrolysis of $ClONO_2$ can occur as the water content of the sulphate aerosol is increased:

$$ClONO_2(g) + H_2O(l) \rightarrow HOCl(g) + HNO_3(g). \qquad (18)$$

The HOCl is then rapidly photolysed, generating Cl. The process therefore has the net effect of converting the reservoir species $ClONO_2$ to active Cl.

4 ClO profiles: models and observations

Many attempts have been made to model ClO mixing ratios. However, modelled [ClO:HCl] concentration ratios consistently exceed those measured for altitudes above about 30 km. Furthermore, in situ measurements of the [ClO:HCl] concentration ratio in the lower stratosphere are at least twice as large as predicted values [7].

Another common characteristic of the models is that they have underestimated the abundance of ozone compared to observations, a phenomenon known as the

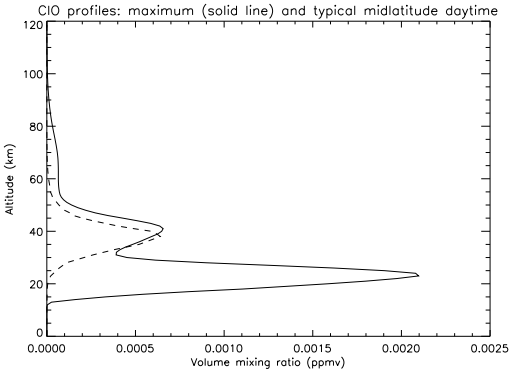

Figure 1: A typical midlatitude day-time ClO profile [10] (dotted line) together with the profile chosen to give a reasonable maximum for the observed mixing ratio of ClO [13] (solid line). This maximum profile corresponds to extremely high ClO levels observed in 'ozone hole' conditions during the Antarctic winter. Note that the midlatitude profile peak is similar to the 'subsidiary peak' displayed by the Antarctic winter profile (see Section 7.2).

'ozone deficit problem'. The discrepancy may be as large as 45% in the upper stratosphere. Also, even recent three-dimensional modelling [9] has overestimated by several times the abundance of ClO.

One of the causes of this discrepancy between models and observations may be the uncertainty in the rate coefficients of the reactions involved.

Since there are still significant gaps in our understanding of the chlorine cycle, we can conclude that it is better to use observed ClO mixing ratios for the purpose of this simulation.

Many such observations have been carried out in the last few years. Moreover, measurements have been made from a variety of platforms, including remote sounding via spectroscopy from ground stations and satellites, as well as whole air sampling form aircraft, balloons and rockets. Recent observations [7] indicate typical midlatitude daytime ClO profiles peaking at about 0.6 ppbv at an altitude of around 35 to 40 km. Such a profile [10] is displayed as the dotted line in Figure 1.

However, since ClO lines are difficult to detect in the infrared spectrum, it is desirable to use an observed profile which corresponds to the maximum occurring mixing ratio of ClO.

Observations [11] show a polar winter ClO profile peaking at a mixing ratio of over 2 ppbv at an altitude of approximately 20 km, with a subsidiary peak at approximately 35 or 40 km. This profile was recorded

over Antarctica in mid August during 'ozone hole' conditions in the southern winter. It is to be expected that maximum ClO levels will be found in polar regions during the winter because PSCs play an important role in controlling levels of ClO (see Section 3.2).

It is interesting to note that although ClO is enhanced over the Arctic too, levels for the northern winter are not nearly as high. This is because the Antarctic winter stratosphere enjoys unique meteorological conditions, being very cold and highly stable. In contrast, the Arctic stratosphere is warmer and much less stable: air masses tend to move in and out of the region every week or two [12]. Moreover, the Arctic vortex breaks down in early spring due enhanced planetary wave activity, whereas the Antarctic vortex does not break down until late spring [8].

Consequently, to simulate a reasonable maximum, a profile has been chosen which corresponds to an Antarctic winter. Such a profile [13] is displayed as the solid line in Figure 1.

Nevertheless, it is also of interest to determine whether it may be possible to observe ClO at midlatitudes from MIPAS. At midlatitudes, ClO has been observed [14] to vary from a nighttime Volume Mixing Ratio (VMR) of almost zero to typical daytime levels of around 0.3–0.6 ppbv. The ClO VMR is almost constant through the middle part of the day, between about 9am and 4pm. This diurnal pattern shows only moderate seasonal variation, peak levels being somewhat higher in the summer and autumn than in the winter and spring.

The sun-synchronous orbit chosen for Envisat-1 (see Section 2) will mean that all its observations are made at approximately 10am and 10pm local time for each region being observed. Therefore, we can expect that MIPAS will encounter daytime midlatitude ClO profiles peaking at levels in the region of 0.6 ppbv.

5 The Reference Forward Model (RFM)

5.1 General Information

The RFM is a line-by-line radiative transfer model, designed to perform reference calculations to be used in the development of MIPAS. It was developed [15] under an ESA contract at AOPP at the University of Oxford, UK.

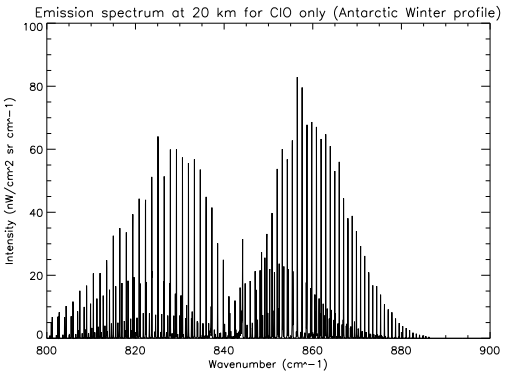

Figure 2: Emission spectrum due to ClO only, based on the VMR profile shown as the solid line in Figure 1. The spectrum is for an altitude of 20 km. There are few other ClO emission features outside this wavenumber region.

5.2 Use of the RFM for modelling the ClO spectrum

In the simulation used here, the RFM models an atmosphere based on the 17 gases which generate the largest contribution to the required emission spectrum. The abundances of the gases correspond to levels typical for the Antarctic winter. 8 gases are simulated 'line-by-line' using the HITRAN line lists, while the remaining 7 are tabulated Cross-Section (XSC) only. The Field-Of-View (FOV) convolution is included to all for the finite size of the interferometer optics.

The simulation calculates spectra and corresponding VMR Jacobians (Weighting Functions) at altitudes from 8 km to 53 km with 3 km resolution: 16 altitudes in all, covering the entire MIPAS scan range.

Preliminary analysis using the RFM showed that the ClO spectrum has significant features only in the region 800 cm^{-1} to 900 cm^{-1}, so only this region of the MIPAS spectrum is considered. A plot of an emission spectrum due only to ClO is shown in Figure 2.

However, even the strongest features of the ClO spectrum tend to be swamped by emissions from other atmospheric gases. The RFM can be run to simulate the contributions due to other gases in the region of interest chosen here. The results of such a simulation are shown in Figure 3.

It may nevertheless be possible to disentangle the ClO spectral contribution from that of other gases. Figure 4 shows the spectral difference between otherwise identical model atmospheres for the case where ClO is present and the case where no ClO is present. Compare

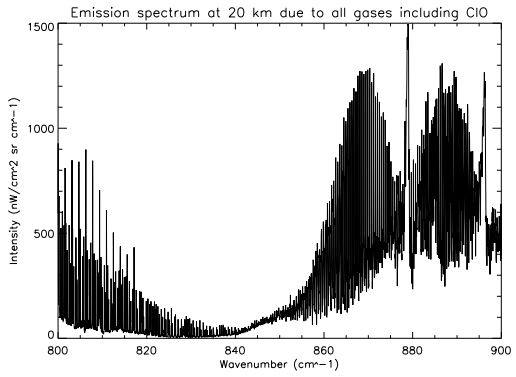

Figure 3: Emission spectrum (again at 20 km) due to the most significant atmospheric gases, including ClO. Pressure and temperature conditions and the gaseous abundances correspond to the Antarctic Winter. By comparison with Figure 2, it is clear that the ClO spectrum is swamped by other spectral contributions.

this with Figure 2, which shows the simulated infrared spectrum from an atmosphere containing only ClO.

A sample RFM 'driver table' is shown in Table 1 [15]. The *FLG section shows that we want to write the Radiance Spectra to `.rad` files (RAD flag), that we want to perform a spectral convolution with the Instrument Line Shape (ILS flag), that Jacobians are to be calculated (JAC flag) and that a Field-Of-View convolution is being applied (FOV flag). The *SPC section identifies the wavenumber region which is of interest for the ClO emission spectrum. The *GAS section identifies the 17 gases to be used in the simulation, while the *ATM section gives the filing locations where data about the atmospheres used in the simulation is held. Tangent heights are listed under *TAN, and *JAC specifies the heights for which Jacobians are to be calculated, both corresponding to the entire MIPAS altitude range. *HIT gives the filing location of the HITRAN line data file, and *ILS gives the location of Instrument Line Shape data. Finally, the *XSC section holds molecular cross-sectional data on 9 of the gases and the *FOV gives the FOV convolution data file.

```
*HDR  ! output file header
28-MAR-00 All gases present
*FLG  ! RFM flags
   RAD ILS JAC FOV
*SPC  ! spectral range and resolution
   800  900 0.025
   ! region of interest for clo
*GAS  ! list of absorbers
   H2O CO2 O3 HNO3 F11 C2H6 OCS
   F22 F12 CCl4 NO2 F113 NH3 F114
   ClONO2 HNO4 ClO
*ATM  ! atmospheric profile
      ! information
   ~dudhia/rfm_files/hgt3km.atm
   ~dudhia/rfm_files/minor.atm
   ! a file of minor gases
   maxclowinprofile
   ! cloprofile from jjr maximum
   ! all other features from Polar
   ! Winter profile
*TAN  ! list of tangent heights
   8 11 14 17 20 23 26 29 32 35
   38 41 44 47 50 53
*JAC  ! list of heights
      ! for Jacobians
   clo 8 11 14 17 20 23 26 29 32
   35 38 41 44 47 50 53
*HIT  ! HITRAN line list
   ~dudhia/rfm_files/hitran_1996.bin
*ILS  ! instrument line shape
      ! convolution
   ~dudhia/rfm_files/ofm.ils
*XSC  ! cross-section files
   ~dudhia/rfm_files/f11.xsc
   ~dudhia/rfm_files/f22.xsc
   ~dudhia/rfm_files/f12.xsc
   ~dudhia/rfm_files/f113.xsc
   ~dudhia/rfm_files/f114.xsc
   ~dudhia/rfm_files/f21.xsc
   ~dudhia/rfm_files/f13.xsc
   ~dudhia/rfm_files/ccl4.xsc
   ~dudhia/rfm_files/clono2.xsc
*FOV  ! field-of-view
   ~dudhia/rfm_files/rfm_1km5.fov
*END
```

Table 1: A sample RFM driver table [15]. Comments are preceded by exclamation marks (!).

6 Theory

6.1 Mathematics of the Retrieval

MIPAS is designed to retrieve the altitude distribution of various gases from limb-scanning observations of the atmosphere; in this case, ClO is being considered. This retrieval requires the fitting of a theoretical model,

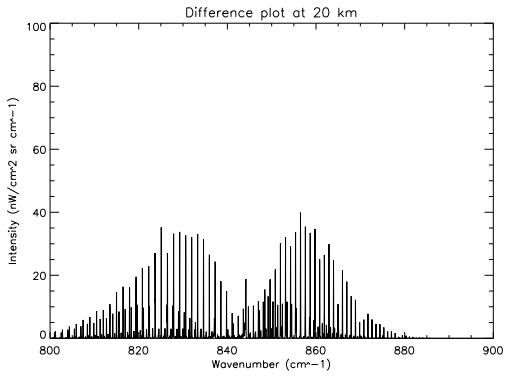

Figure 4: A plot showing the difference between the simulated infrared spectrum for two atmospheres, the first of which contains ClO and the second of which does not. The atmospheres are identical in every other respect and correspond to Antarctic Winter conditions. The plot is for an altitude of 20 km. The gases used in the simulations are those given in the *GAS section of the RFM driver table in Table 1. The scale is the same as that of Figure 2 so that they can be readily compared. Note the reduction by a factor of approximately 2.

describing the radiance of the atmosphere under certain parameters, to the observations. The theoretical model simulates the observations using parameters of two types: those that are not retrieved by MIPAS but that still affect the atmospheric radiance, and those that are retrieved, namely information about the distribution of ClO. The retrieval process consists of searching for the set of values for the ClO distribution that generates the best simulation for the observations [16].

Therefore, if we choose a particular Volume Mixing Ratio (VMR) profile for ClO, then we can run the RFM to calculate a simulation for the radiance measurement which will be produced at a particular tangent height and wavenumber. We can express the value or values calculated in this way several forms:

1. Single measurement (y), single level (x).

$$\mathrm{y} = \mathrm{k}\mathrm{x} + \epsilon \tag{19}$$

   where y, k, x and ϵ are all scalars. y is a single observed measurement, k is the Jacobian dy/dx, x is a single value of the VMR and ϵ is some unknown random error representing the noise on the measurement. ϵ has a mean of zero and a standard deviation equal to σ_{y}. In this case, we can find an exact solution trivially: x=y/k where $\sigma_{\mathrm{x}}^2 = \sigma_{\mathrm{y}}^2/\mathrm{k}^2$.

2. Spectrum (**y**), single level (x).

$$\mathbf{y} = \mathbf{k}\mathrm{x} + \boldsymbol{\epsilon} \tag{20}$$

   where **y**,**k** and $\boldsymbol{\epsilon}$ are column vectors and x is a scalar. This notation allows us to express several results in a more compact form.

   This time, in order to find the best fit between the spectrum and the **k**x values, we calculate a least squares fit: *i.e.* there is no exact solution. This is equivalent to minimising $(\mathbf{y} - \mathbf{k}\mathrm{x})^T(\mathbf{y} - \mathbf{k}\mathrm{x})$ as we vary x:

$$\begin{aligned} \frac{\partial}{\partial \mathrm{x}}((\mathbf{y} - \mathbf{k}\mathrm{x})^T(\mathbf{y} - \mathbf{k}\mathrm{x})) &= 0 && (21)\\ -2\mathbf{k}^T(\mathbf{y} - \mathbf{k}\mathrm{x}) &= 0 && (22)\\ -\mathbf{k}^T\mathbf{y} + \mathbf{k}^T\mathbf{k}\mathrm{x} &= 0 && (23)\\ \mathrm{x} = (\mathbf{k}^T\mathbf{k})^{-\mathbf{1}}\mathbf{k}^T\mathbf{y}. && (24) \end{aligned}$$

   We can now consider the row matrix **d** where $\mathbf{d} = (\mathbf{k}^T\mathbf{k})^{-1}\mathbf{k}^T\mathbf{y}$. If we assume that the noise is uncorrelated, then we can write the noise covariance in the form $\mathbf{S}_{\mathrm{y}} = \sigma_{\mathrm{y}}^2\mathbf{I}$ where **I** is the identity matrix. Since $\mathrm{x} = \mathbf{d}\mathbf{y}$, this leads to the relation

$$\begin{aligned} \sigma_{\mathrm{x}}^2 &= \mathbf{d}\sigma_{\mathrm{y}}^2\mathbf{I}\mathbf{d}^T && (25)\\ &= \sigma_{\mathrm{y}}^2(\mathbf{d}\mathbf{d}^T). && (26) \end{aligned}$$

3. Apodisation and correlated noise.

   The apodisation can be expressed in the form $\mathbf{y} = \mathbf{A}\mathbf{y}'$ where **y** is the apodised spectrum and $\mathbf{y}'$ is unapodised. The covariance matrix $\mathbf{S}_{\mathrm{y}}$ is now no longer diagonal:

$$\mathbf{S}_{\mathrm{y}} = \mathbf{A}\sigma_{\mathrm{y}}^2\mathbf{I}\mathbf{A}^T. \tag{27}$$

   This time, the least squares fit is obtained by minimising $\chi^2 = (\mathbf{y} - \mathbf{k}\mathrm{x})^T\mathbf{S}_{\mathrm{y}}^{-1}(\mathbf{y} - \mathbf{k}\mathrm{x})$ which leads to the results

$$\mathrm{x} = \mathbf{d}\mathbf{y} = (\mathbf{k}^T\mathbf{S}_{\mathrm{y}}^{-1}\mathbf{k})^{-1}\mathbf{k}^T\mathbf{S}_{\mathrm{y}}^{-1}\mathbf{y} \tag{28}$$

   and

$$\begin{aligned} \sigma_{\mathrm{x}}^2 &= (\mathbf{d}\mathbf{S}_{\mathrm{y}}^{-1}\mathbf{d}^T)^{-1} && (29)\\ &= (\mathbf{k}^T\mathbf{S}_{\mathrm{y}}^{-1}\mathbf{k})^{-1}. && (30) \end{aligned}$$

4. Whole profile retrieval.

$$\mathbf{y} = \mathbf{K}\mathbf{x} + \boldsymbol{\epsilon} \tag{31}$$

   where **y**, **x** and $\boldsymbol{\epsilon}$ are column vectors and **K** is a matrix. This allows us to express the results from several profile levels compactly. Instead of the scalar

variance σ_x^2 we now have $\mathbf{S}_x$, the error covariance matrix of $\mathbf{x}$. From the previous section, we have at once that

$$\mathbf{S}_x = (\mathbf{K}^T \mathbf{S}_y^{-1} \mathbf{K})^{-1}. \quad (32)$$

The initial MIPAS spectrum is unapodised, so noise is uncorrelated. We 'apodise' the spectrum to reduce interferogram edge effects, but that process also introduces correlations in the noise.

6.2 Accuracy available on individual VMR measurements

Consider the direct retrieval of a single value of the VMR from a single value of observed radiance. We would then have

$$y = K'v \quad (33)$$

where y is the radiance, v is the VMR and K' is equal to δ(radiance)/δ(unit increase in VMR). In order to find $K' = \delta y/\delta v$, we would increase v by some constant amount (for example, δv = 0.01 ppmv) and calculate the difference in radiance, δy. In this case, K' would then be multiplied by 100 to convert to a unit (ppmv) increase in v.

However, this method may encounter difficulties if the VMR varies over a large range: a small perturbation at one point may be a very large perturbation at another. For this reason, we instead increase v by some *fraction*, for example δv = 0.01v. If we multiply the radiance difference by 100 then we have K = δ(radiance)/δ(unit fractional increase in VMR).

Now δ(fractional increase in VMR) = $\delta v/v = \delta(\ln v)$, so the units of retrieval are $x = \ln v$ since the units of K determine the units of the retrieved quantity. This means that we retrieve $x + \sigma_x$, and to find the VMR uncertainty, we have

$$v = \exp(x) \quad (34)$$

$$v + \sigma_v = \exp(x + \sigma_x). \quad (35)$$

Dividing Equation 35 by Equation 34 gives

$$1 + \frac{\sigma_v}{v} = \exp(\sigma_x) \quad (36)$$

which leads to the result

$$\sigma_v = v(\exp(\sigma_x) - 1). \quad (37)$$

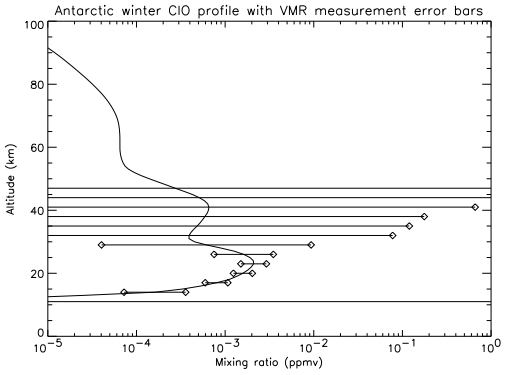

Figure 5: Error bars on VMR measurements approximated using a diagonalised $\mathbf{S}_y$ matrix. The profile used is that corresponding to maximum ClO levels, occurring in the Antarctic winter. The bars are of reasonable size in the region around 20 km, but elsewhere far too large for any useful measurements to be made.

7 Analysis

7.1 Simplified analysis

It is useful to start with a simplified analysis to find an approximation to the final results. To do this, we ignore apodisation (and therefore noise correlation). This is equivalent Case 2 in Section 6.1, where σ_y^2 is the uncorrelated noise. We also consider one tangent height at a time.

We begin by finding the value of σ_y: in the region of interest for ClO features, wavenumbers 800 to 900 cm^{-1}, the NESR (or σ_y) is approximately equal to 25 nW/cm^{-2} sr cm^{-1} [17]. It should of course be noted that the errors we go on to obtain using this NESR should be regarded as *minimum* values because other errors have been neglected. These other possible sources of error include inaccurate spectroscopic data, errors in the temperature profile and other species concentrations as well as imprecise knowledge of the instrument performance in such areas as calibration, instrument line shape or pointing information.

It is straightforward to calculate a series of error bars for the profile. We use Equation 37 to calculate the fractional profile error (σ_v) at each MIPAS scan altitude.

The results from such a procedure have been plotted as error bars on the logarithmic plot in Figure 5. Notice that the error bars are of equal length on each side of the profile curve in logarithmic space (as expected from Section 6.2).

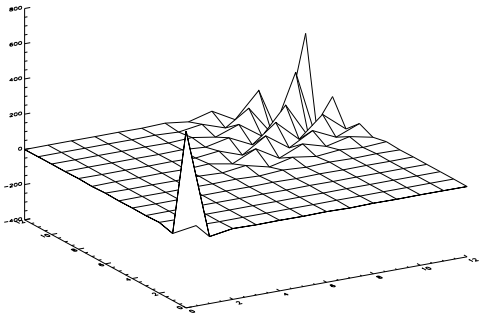

Figure 6: A surface representing the error covariance matrix $\mathbf{S_x}$. The vertical axis represents the variance and the other two axes give respectively the height at which the perturbation is applied and the height at which the VMR measurement is made. In this case, the indices 0,1,...,12 correspond to altitudes 8,11,...47 km. Note that the matrix is symmetric about the leading diagonal and that the smallest errors occur in the region around 20 km, as shown in the error bars in Figures 7 and 8.

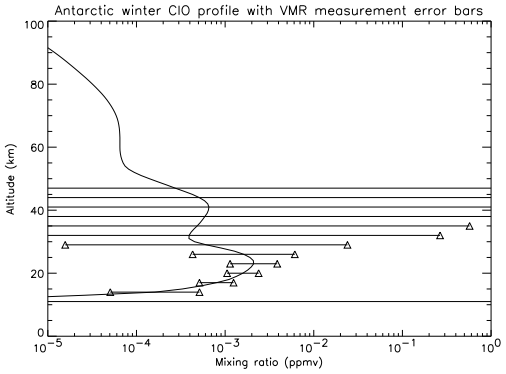

Figure 7: VMR error bars for full retrieval analysis: non-diagonalised $\mathbf{S_y}$, with apodisation and noise correlation corrections.

7.2 Full analysis

To carry out the full analysis, we must include apodisation and therefore also allow for noise correlation effects. This is equivalent to Case 4 in Section 6.1. We can expect the results to be similar to those already found using the simplified analysis in Section 7.1.

Including the apodisation and noise correlation corrections and performing the full multiple-layer retrieval analysis, we obtain the covariance matrix $\mathbf{S_x}$. A surface corresponding to $\mathbf{S_x}$ is shown in Figure 6. By considering the diagonal elements, we find larger VMR error bars than before, as is displayed in Figure 7. A close-up of the region in which the error bars are of a reasonable size is shown in Figure 8. The figure displays error bars before and after the corrections have been applied.

We are now in a position to use the error bar plots to determine whether or not MIPAS will be able to make useful measurements of ClO. It would appear from Figure 8 that during 'ozone hole' Antarctic winter conditions ClO may be sufficiently abundant for information to be retrieved. Useful retrieval is however restricted to a narrow altitude range in which the ClO VMR peaks. Typical errors bars at an altitude of 20 km are found to be $\sim$50%. Error bars at 17km are similar and those at 23km increase to $\sim$80%. Outside this region, error bars are very large and no retrieval can practicably be made.

We can also consider the possibility of ClO profile retrieval for typical midlatitude conditions. However,

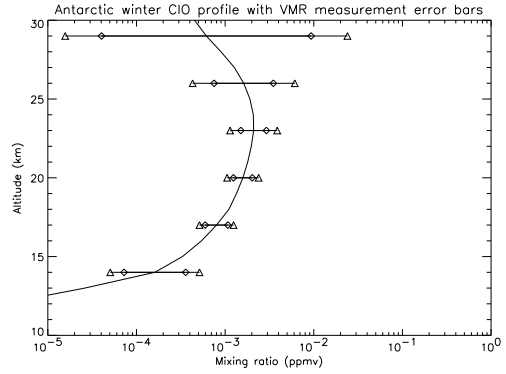

Figure 8: A close-up of the error bars shown in Figure 7 (triangles) together with the error bars for the single-layer retrieval analysis shown in Figure 5 (lozenges). Notice that the error bars are somewhat larger after the apodisation and noise correlation corrections have been applied. The close-up is shown for the region in which the error bars are of a reasonable size.

as Figure 1 shows, the midlatitude ClO VMR peaks at an altitude of approximately 40 km, and is very similar to the subsidiary peak displayed by the Antarctic winter ClO profile. Since we have already seen from the Antarctic winter profile that the error bars in the vicinity of this subsidiary peak are very large (see Figure 7), we can deduce that there is no prospect of useful midlatitude ClO measurements being made.

8 Conclusion

During normal midlatitude stratospheric conditions, ClO is not sufficiently abundant for profile information to be usefully retrieved by MIPAS.

However, according to observed ClO profiles, ClO is much more abundant during Antarctic winter conditions. It should therefore be possible to use MIPAS to obtain information about ClO profiles in these conditions, but only in a restricted altitude range, probably $\sim$17–23 km. Even in this region, typical error bars are $\sim$50–80%. It may be possible to achieve improved accuracy by averaging a number of single spectra, although this would be at the expense of reduced spatial and temporal resolutions. At other tangent altitudes, the simulations show that the error bars are large, much too large for any useful ClO profile information to be retrieved.

References

[1] Ruhnke, R. *et al.*, 'The vertical distribution of ClO at Ny-Ålesund during March 1997', *Geophys. Res. Lett.* **26**, 839–842.

[2] Del Negro, L. A. *et al.*, 'Comparison of modeled and observed values of NO_2 and JNO_2 during the Photochemistry of Ozone Loss in the Arctic Region in Summer. (POLARIS) mission', *J. Geophys. Res.—Atm.* **104**, 26687–26703.

[3] von Clarmann, T. *et al.*, '$ClONO_2$ vertical profile and estimated mixing ratios of ClO and HOCl in winter Arctic stratosphere from Michelson interferometer for passive atmospheric sounding limb emission spectra', *J. Geophys. Res.—Atm.* **102**, 16157–16168.

[4] Waters, J. W. *et al.*, 'Validation of UARS Microwave Limb Sounder ClO measurements', *J. Geophys. Res.—Atm.* **101**, 10091–10127.

[5] Echle, G. *et al.*, 'On the potential of i.r. limb emission spectroscopy for the measurement of the stratospheric composition', *J. Quant. Radiat. Transfer* **52**, 253–265.

[6] ESA website: http://envisat.estec.esa.nl/.

[7] *Atmospheric Chemistry and Global Change*, G. P. Brasseur, J. J. Orlando, G. S. Tyndall (editors) (Oxford University Press, 1999).

[8] Henderson, G. S. *et al.*, 'Polar ozone depletion: Current status', *Can. J. Phys.* **69** 1110–1122.

[9] Khosravi, R. *et al.*, 'Significant reduction in the stratospheric ozone deficit using a three-dimensional model constrained with UARS data', *J. Geophys. Res.—Atm.* **103**, 16203–16219.

[10] von Clarmann, T. *et al.*, 'Study on the simulation of atmospheric infrared spectra', *ESA* 1998.

[11] Waters, J. W. *et al.*, 'Validation of UARS Microwave Limb Sounder Measurements', *J. Geophys. Res.—Atm.* **101**, 10091–10127.

[12] Rowland, F. S., 'Stratospheric Ozone Depletion by Chlorofluorocarbons', *Ambio. (Stockholm)* **19**, 281–292.

[13] Profile by J. J. Remedios (AOPP, University Of Oxford, UK).

[14] Ricaud, P. *et al.*, 'Temporal evolution of chlorine monoxide in the middle stratosphere', *J. Geophys. Res.* **105**, 4459–4469.

[15] RFM information from the website http://www.atm.ox.ac.uk/RFM.

[16] Ridolfi, M. *et al.*, 'Optimized forward model and retrieval scheme for MIPAS near-real-time data processing', *App. Opt.* **39**, 1323–1340.

[17] ESA: NESR data from the first MIPAS TV performance test campaign.